land

MDPI

Article

Mapping of Forest Species Using Sentinel-2A Images in the Alentejo and Algarve Regions, Portugal

Crismeire Isbaex [1,*], Ana Margarida Coelho [2], Ana Cristina Gonçalves [3] and Adélia M. O. Sousa [4]

[1] MED—Mediterranean Institute for Agriculture, Environment and Development & CHANGE—Global Change and Sustainability Institute, Institute for Advanced Research and Training, University of Évora, P.O. Box 94, 7002-544 Évora, Portugal
[2] ICT—Institute of Earth Sciences, Institute for Advanced Research and Training, Colégio Luis António Verney, Rua Romão Ramalho, University of Évora, 59, 7002-554 Évora, Portugal; ana.coelho@certis.pt
[3] MED—Mediterranean Institute for Agriculture, Environment and Development & CHANGE—Global Change and Sustainability Institute, Institute for Advanced Research and Training, Rural Engineering Department, School of Science and Technology, University of Évora, P.O. Box 94, 7002-544 Évora, Portugal; acag@uevora.pt
[4] MED—Mediterranean Institute for Agriculture, Environment and Development & CHANGE—Global Change and Sustainability Institute, Institute for Advanced Research and Training, Remote Sensing Laboratory—EaRSLab, Rural Engineering Department, School of Science and Technology, University of Évora, P.O. Box 94, 7002-544 Évora, Portugal; asousa@uevora.pt
* Correspondence: cisbaex@uevora.pt

Abstract: Land use and land cover (LULC) studies, particularly those focused on mapping forest species using Sentinel-2 (S2A) data, face challenges in delineating and identifying areas of heterogeneous forest components with spectral similarity at the canopy level. In this context, the main objective of this study was to compare and analyze the feasibility of two classification algorithms, K-Nearest Neighbor (KNN) and Random Forest (RF), with S2A data for mapping forest cover in the southern regions of Portugal, using tools with a free, open-source, accessible, and easy-to-use interface. Sentinel-2A data from summer 2019 provided 26 independent variables at 10 m spatial resolution for the analysis. Nine object-based LULC categories were distinguished, including five forest species (*Quercus suber*, *Quercus rotundifolia*, *Eucalyptus* spp., *Pinus pinaster*, and *Pinus pinea*), and four non-forest classes. Orfeo ToolBox (OTB) proved to be a reliable and powerful tool for the classification process. The best results were achieved using the RF algorithm in all regions, where it reached the highest accuracy values in Alentejo Central region (OA = 92.16% and K = 0.91). The use of open-source tools has enabled high-resolution mapping of forest species in the Mediterranean, democratizing access to research and monitoring.

Keywords: machine learning; supervised classification; mediterranean; random forest; k-nearest neighbor

Citation: Isbaex, C.; Coelho, A.M.; Gonçalves, A.C.; Sousa, A.M.O. Mapping of Forest Species Using Sentinel-2A Images in the Alentejo and Algarve Regions, Portugal. *Land* **2024**, *13*, 2184. https://doi.org/10.3390/land13122184

Academic Editors: Todd Robinson and Dailiang Peng

Received: 22 October 2024
Revised: 9 December 2024
Accepted: 11 December 2024
Published: 14 December 2024

1. Introduction

Mapping changes in land use and land cover (LULC) is essential for understanding ecosystem dynamics and ensuring sustainable natural resource management. Several methods and techniques have been used, among which are those linked to remote sensing, especially with Sentinel-2 data. Mapping LULC is a challenge when landscape has large variability and fragmentation, such as in the Mediterranean region [1]. The main land use classes in continental Portugal are forest (36%), woods and pastures (31%), agricultural areas (24%), urban use (5%), unproductive (2%), and inland waters (2%) [2]. Considering the aforementioned, it is pivotal to study the potentiality of remote sensing data to map Mediterranean ecosystem. This will enable us to map forest species distribution. For these reasons, maps serve as an intermediate step in more complex analyses such as landscape modeling, estimating forest biomass, and environmental monitoring [3,4]. In addition to being a region prone to forest degradation and wildfire, as is the case for many

Mediterranean forests [5,6], the forest species' identification and spatial distribution are essential to monitoring biodiversity, climate change, and forest management.

Remote sensing has undergone significant changes in recent years, resulting in a substantial increase in both the temporal frequency and spatial resolution of satellite imagery, as well as improved data accessibility. Several satellite types are available on open-access platforms, including high-resolution satellite imaging systems (Friedl et al. [7]), and several non-commercial software packages have image analysis tools [8–10].

Sentinel-2A (S2A) is a multispectral sensor (MSI) which has a five-day revisit time, high spatial resolution and its data are open sourced [11]. It is composed of 13 spectral bands, with a wavelength between 443 and 2190 nm, ranging from the visible spectrum, vegetation red-edge bands (Red-edge), near-infrared (NIR), narrow infrared (Narrow NIR), and shortwave infrared (SWIR) [11]. Depending on the band, three spatial resolutions are available: 10 m (B2, B3, B4 (V), and B8 (NIR)), 20 m (B5, B6, B7, (Red-edge), B8a (Narrow NIR), B11 and B12 (SWIR)), and 60 m (B1, B9, and B10). The S2A product can be acquired with corrected reflectance images at the base of the atmosphere and the closest ground measurements (Bottom Of Atmosphere—BOA) [12]. S2A when compared to Landsat mission and MODIS data have the advantage of having more spectral bands and higher spatial resolution, respectively [13].

In addition to spectral information from Sentinel-2 bands, vegetation and texture indices are widely used in remote sensing to improve LULC classification and forest mapping [14,15]. These indices provide complementary information to the spectral band wavelengths, enabling more accurate identification and mapping of Mediterranean vegetation types and different types of land cover. Vegetation indices are a type of spectral indices that specifically target the reflectance properties of vegetation. These indices are calculated using the red and near-infrared bands of a satellite image and can be used to estimate vegetation biomass, health, and productivity. In particular, vegetation indices, such as Green Normalized Difference Vegetation Index (GNDVI), Soil-Adjusted Vegetation Index (SAVI), Enhanced Vegetation Index (EVI), Normalized Difference Infrared Index (NDII), Normalized Difference Vegetation Index red-edge 1 narrow (NDRE 1), Normalized Difference Vegetation Index red-edge 2 narrow (NDRE 2), and Red-edge Chlorophyll Index (CI), can be used to discriminate different vegetation types [16,17]. Their advantage is related to being sensitive to patterns, especially in semi-arid environments [18].

Texture indices refer to the spatial arrangement of different land cover types within an image. They are calculated by analyzing the variation in pixel values within a local neighborhood of the image. These indices can be used to identify patterns in the landscape that are not easily discernible from color imagery alone [19]. For LULC classification purposes, the texture measurements of a Gray Level Co-occurrence Matrix (GLCM), proposed by Haralick et al. [20], provide further information, which allows us to classify heterogeneous land uses that spectral information is not able to differentiate [19], which is why it is a widely used method. The GLCM method analyzes the existing co-occurrences between each pair of pixels in an image; that is, it analyzes the spatial relationship between a set of pixels (given a distance and different angles) [20–22]. GLCM, being not related to spectral data, frequently attains higher image classification accuracy [1,23,24]. The GLCM texture index can be used to identify areas with high or low levels of spatial heterogeneity, which can be useful for distinguishing between different forest types [25,26]. Principal component analysis (PCA) is one of the commonly used methods to calculate GLCM textures from spectral bands or vegetation indices [18,22], with the goal of simplifying and reducing the number of explanatory variables and the correlation between them [27,28].

In the supervised classification method, training selection and classification methods are also crucial steps in accurately mapping forest classes using satellite data. The quality of the training samples and the appropriateness of the classification method used determine the accuracy of the final forest classification map [29,30]. In recent decades, methods based on machine learning, non-parametric methods, have been frequently applied in remote sensing [31,32], such as K-Nearest Neighbor (kNN) [33] and Random Forest (RF) [34]. kNN

is a non-parametric learning method proposed by Wettschereck et al. [35]. It does not make assumptions about the training dataset, since it is independent of the data spectral distribution [36]. In this way, kNN is based on a calibration dataset, where it finds a set of k training samples closest to the unknown samples, frequently based on the Euclidean distance function [36–39]. Random Forest (RF), proposed by [34], divides datasets into two subsets (i.e., training and validation). The method is based on the definition of decision trees with random bootstrapping of training data, which, inversely to the decision tree (DT) method, does not have overfitting problems [40,41]. A random subset of predictors is used at each node to divide the tree into decision trees. The output is the mean of all decision trees, based on the majority of "votes" per class (unweighted) [42,43].

These methods perform well in data categorization where input complexity is high, and they are widely accepted in LULC mapping [4,43–46]. Several studies compared different classification algorithms to classify LULC with Sentinel-2 data. The RF algorithm was compared with other commonly used classification methods, including Maximum Likelihood (ML), support vector machine (SVM), and KNN [30,47,48]. For all studies, the RF algorithm presents better results in terms of overall accuracy, kappa coefficient, and user accuracy. The authors discussed the importance of selecting appropriate training samples and choosing the appropriate classification method for a particular forest type to ensure accurate classification. More information on supervised classification methods can be found in [49].

In particular, the Mediterranean ecosystem presents a unique set of challenges due to its complex vegetation patterns, topography, and land use changes. In these ecosystems, where there is great structural and botanical diversity with high spectral variability [50], supervised classification methods based on machine learning algorithms have attracted attention for being able to deal with large volumes of complex and non-parametric data [43,51]. For Mediterranean systems, some studies have been developed to obtain LULC maps with Sentinel-2 data, in Mediterranean ecosystems in Greece [52], Spain [53,54], Tunisia [55], and Italy [46]. These studies compared RF with other classification algorithms such as Convolutional Neural Networks (CNNs), support vector machines (SVMs), Multilayer Perceptron, Maximum Likelihood, K-Dimensional Trees K-Nearest Neighbors (KDTree-KNNs), Minimum Distance Classification (MDC), and classification and regression tree (CART). The results for these studies showed that RF achieved the highest classification accuracy, with overall accuracy higher than 88%. The RF algorithm is a popular choice for remote sensing applications and is the main objective due to its ability to handle large datasets, reduce overfitting, and provide accurate and interpretable results.

This study presents a LULC mapping approach entirely developed in an open-source environment, aiming to explore its potential for collecting sampling data and classifying high-resolution images from Sentinel-2. In the supervised classification, the Orfeo ToolBox (OTB) version 6.6.1 is an application available in the open-source since software QGIS version 3.8 through a Python plugin [56]. The OTB has specific characteristics suitable for spatial data analysis and high-resolution image processing [57]. This open-source project receives regular updates from the open-source geospatial community, ensuring its relevance in studies such as vegetation monitoring [58]. Its compatibility with various remote sensing data formats, including Sentinel-2 images, increases its versatility and applicability in supervised classification [58]. A significant advantage of OTB is its accessibility through the software QGIS plugin, allowing researchers and professionals with limited programming knowledge to use advanced supervised classification tools. OTB is composed of several classification algorithms, such as Random Forests and K-Nearest Neighbors (KNNs), and processes large data at scale [56]. Furthermore, this approach enabled the exploitation of the strengths of supervised classification without the need for advanced programming knowledge, which optimized the acquisition of a high-precision forest cover map.

The significant contribution of this research lies in the proposed workflow for analyzing different image datasets from Sentinel-2 satellite and variables with vegetation and texture indices, aiming to enhance the classification accuracy of forest species in southern

Portugal. This study addresses the application of machine learning to detect the main challenges in generating high-precision, large-scale classified LULC maps in highly complex forested landscapes. These landscapes are characterized by mixed forest compositions and a heterogeneous, fragmented, and dispersed spatial pattern. The methodological approach focuses on demonstrating the possibility of creating precise maps using open-source tools and data, making the methodology democratically accessible. The proposal aims to achieve scientific reproducibility in LULC mapping studies, enabling access for university students, professionals, and GIS enthusiasts with basic knowledge, thus promoting the dissemination of geospatial knowledge. To enhance the accessibility of analysis, classification, and mapping processes for different users with diverse backgrounds and varying software and hardware availability, the main objectives of this study were as follows: (i) to produce a mapping of forest species cover in the Alentejo and Algarve regions, southern Portugal, using remote sensing data derived from the Sentinel-2 (S2A) satellite; (ii) to develop a methodology and evaluate and compare the feasibility of KNN and RF classification algorithms in S2A; (iii) to use free and open-source data and image analysis tools, focusing on accessibility for users without advanced programming knowledge, offering a user-friendly interface and the ability to process large datasets; (iv) to use the open-source QGIS and SNAP software and the OTB plugin, an image processing library, to classify and analyze Sentinel-2 (S2A) data.

2. Materials and Methods

2.1. Study Area

The study area covers NUT II (NUT—Nomenclature of Territorial Units for Statistical Purposes), Alentejo (AL) and Algarve (AG) [59]. The Alentejo is divided into four NUT III, namely Alto Alentejo (AA), Alentejo Central (AC), Alentejo Litoral (AL), and Baixo Alentejo (BA) (Figure 1) [59]. These regions are located in the southern mainland of Portugal, with a total territorial extension of 36 602 km^2, with a Mediterranean climate, with hot and dry summers (June to September) and cold and rainy winters (October to January). Total forest area is about 1,270,000 ha, and the most representative species in terms of area are *Quercus suber*, *Quercus rotundifolia*, *Eucalyptus* spp., *Pinus pinea*, and *Pinus pinaster* [2].

Quercus suber, *Quercus rotundifolia,* and *Pinus pinea* occupy the largest share of the forest area and are managed as agroforestry systems [60], which have low density, heterogeneous spatial distribution, in pure stands or mixed with other species, and usually shrub and herbaceous species in the understory [61–64]. *Eucalyptus* spp. and *Pinus pinaster* are managed as forest systems for timber [65,66] and have higher density and more homogenous spatial distribution than the former [64].

2.2. Data Processing and Dataset

The methodology for the satellite image processing is outlined in Figure 2, which includes the main following steps: (1) selection of Sentinel-2 image processing, calculation of vegetation indices, and calculation of the principal component analysis (PCA) and the GLCM textures (cf. Section 2.3); (2) definition of training and test samples; (3) application of the supervised classification algorithms (cf., Section 2.4.1); and (4) accuracy assessment of different classifiers on a test set using the confusion matrix (cf., Section 2.4.2).

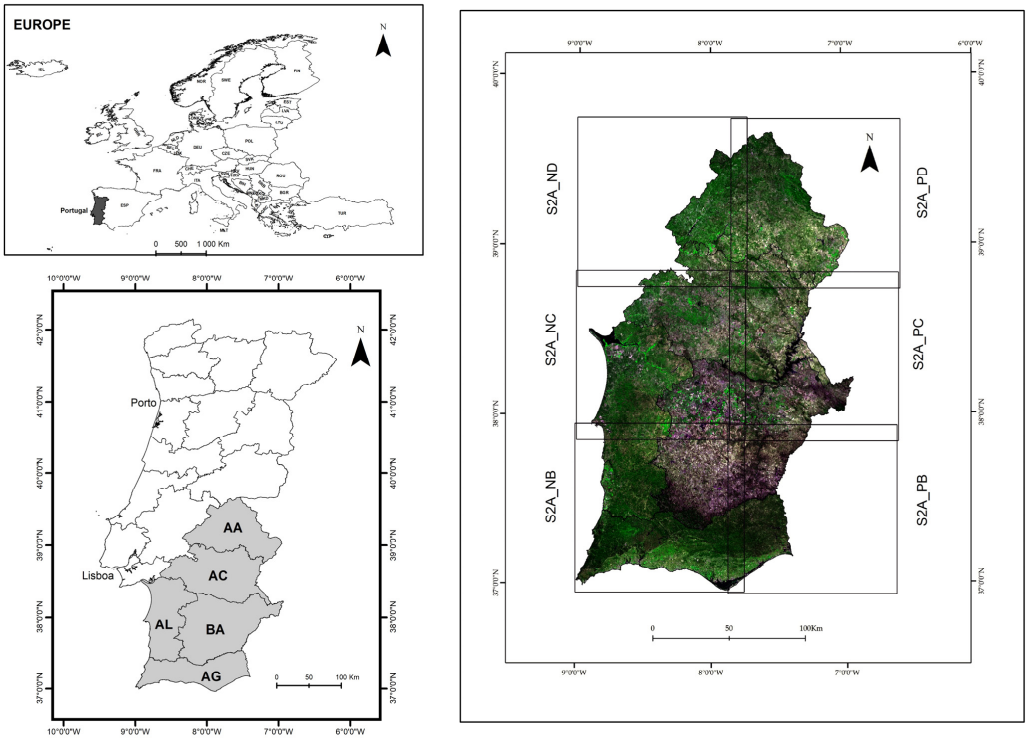

Figure 1. On the left, a location map of Portugal and the study area with the NUTS III administrative division, where AA means Alto Alentejo, AC means Alentejo Central, AL means Alentejo Litoral, BA means Baixo Alentejo, and AG means Algarve. On the right, it shows the false-color composite using the Red, Green, and Blue (RGB) channels, corresponding to Bands 4, 8, and 3, using Sentinel-2A images, and the mosaic of the six images used in this study, named S2A_NB, S2A_NC, S2A_ND, S2A_PB, S2A_PC, and S2A_PD.

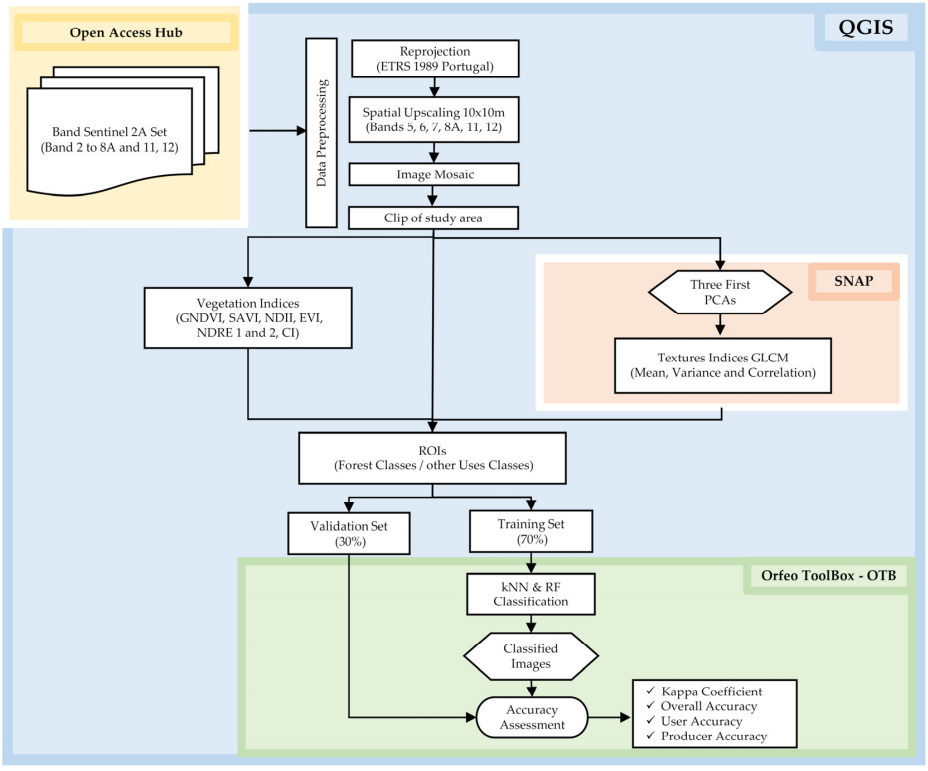

Figure 2. Workflow of the data processing and validation steps implemented from Sentinel-2A images.

2.3. Spectral Data

Copernicus Open Access Hub platform [11] was used to acquire S2A images. The image product used was the atmospherically corrected surface reflectance, Level 2A, derived from the associated Level 1C product, radiometrically corrected imagery. To cover the entire study area (Figure 1 right), six S2A images were used (approximately 1 GB each file) with the same date acquisition (2 September 2019) and cloud filtering of less than 10%. In this study, 10 S2A Multispectral (MSI) reflectance bands were used (B2, B3, B4, B5, B6, B7, B8, B8A, B11, and B12); the mosaics per reflectance band were set in European Terrestrial Reference System 1989 (ETRS 1989). The summer season was selected because, in the Mediterranean environment, the probability to find images with a lower percentage of cloud cover and contrast between the spectral signature of the different forest species and the understory vegetation is larger [18,67]. To obtain all bands with the same spatial resolution, spatial upscaling using the nearest neighbor method was applied to convert the 20m bands (5, 6, 7, 8A, 11, and 12) into 10m spatial resolution [68].

Seven vegetation indices (VIs) and nine texture indices (Gray Level Co-occurrence Matrix—GLCM) were implemented to promote spectral discrimination of forest classes (Table 1). This approach became necessary due to the intrinsic limitations of broad spectral bands, such as their susceptibility to atmospheric interference and the resulting similar spectral reflectance patterns in different vegetation types [50,69]. Traditional VIs, as well as some more recent VIs utilizing red-edge spectral bands available in Sentinel-2 data, were employed to contribute to better separability of land use and land cover (LULC) classes, with an emphasis on vegetation classes. The processing of Sentinel imagery and the calculation of vegetation indices (VIs) were performed using QGIS 3.16.0-Hannover software.

Principal component analysis was applied to the set of 10 Sentinel-2A spectral bands, following recommendations from various studies [27,70,71]. In this study, the first three principal components were selected for subsequent analysis, as they explained more than 97.10% of the spectral variation of the dataset for all regions (Table 2). This approach is based on the premise, corroborated by previous research [1,22,72], that the first three principal components retain most of the relevant information for discriminating land use and land cover classes.

From these three principal components, each GLCM texture measure (Average—MEA, Variance—VAR, and Correlation—COR) was calculated using a 9 × 9 pixel moving window in the 0°, 45°, 90°, and 135° directions of 32 gray levels, with the variogram method [73]. The size of the moving window depends on the land use characteristics and the diversity of the bands [50,74]. Szantoi et al.'s [75] window size was adapted due to its ability to evaluate heterogeneous regions, regardless of the size of the training features. GLCM textures were generated using SNAP (Sentinel Application Platform) software version 7 [75]. In this study, the selection of vegetation and texture indices was based on their demonstrated performance in previous research [76–78]. In total, the input dataset for this study comprised 26 independent variables.

Table 1. Description and formula of the indices.

Types		Descriptions	Equations
Vegetation Indices * (VIs)	GNDVI [79]	Green Normalized Difference Vegetation Index	$\frac{B8-B3}{B8+B3}$
	SAVI [80]	Soil-Adjusted Vegetation Index	$1.5 \times \frac{B8-B4}{8\times(B8+B4+0.5)}$
	NDII [81]	Normalized Difference Infrared Index	$\frac{B8-B11}{B8+B11}$
	EVI [82]	Enhanced Vegetation Index	$2.5 \times \left(\frac{B8-B4}{(B8-6\times B4-(B4-7.5\times B2)+1)}\right)$
	NDRE 1 [83]	Normalized Difference Red Edge Index 1	$\frac{B8A-B5}{B8A+B5}$
	NDRE 2 [83]	Normalized Difference Red Edge Index 2	$\frac{B8A-B7}{B8A+B7}$
	CI [84]	Red-edge Chlorophyll Index	$\frac{B6}{B5}$

Table 1. *Cont.*

Types	Descriptions		Equations
Textures **	Gray-level co-occurrence matrix (GLCM) [20]	MEA	$\sum_{i,j=0}^{N-1} i\ P_{i,j}$
		VAR	$\sum_{i,j=0}^{N-1} iP_{i,j}\ (i-\mu)^2$
		COR	$\frac{\sum_{i,j=0}^{N-1} iP_{i,j} - \mu_x\ \mu_y}{\sigma_x\ \sigma_y}$

* where the central wavelength (µm): *B*2 (490), *B*3 (560), *B*4 (665), *B*5 (705), *B*6 (740), *B*7 (783), *B*8 (842), *B*8*A* (865), *B*11 (1610), and *B*12 (2100). ** where $P(_{i,j})$ is a normalized gray-tone spatial dependence matrix such that SUM(i,j = 0, $N-1$) ($P(_{i,j})$) = 1; *i* and *j* represent the rows and columns, respectively, for the measures of Mean, Variance and Correlation; µ is the mean, for the Variance textural measure; and *N* is the number of distinct gray levels in the quantized image; μ_x. μ_y, σ_x, and σ_y are the means and standard deviations of p_x (sum of each row in co-occurrence matrix) and p_y (sum of each column in the co-occurrence matrix), respectively.

Table 2. Cumulative values of principal component (PC) eigenvalues.

NUTIII Regions	AA	AC	AL	BA	AG
PC1	77.69%	96.87%	75.64%	81.60%	95.77%
PC1 + PC2	93.16%	98.81%	92.99%	93.15%	98.24%
PC1 + PC2 + PC3	97.18%	99.78%	97.42%	97.10%	99.45%

where AA—Alto Alentejo, AC—Alentejo Central, AL—Alentejo Litoral, and BA—Baixo Alentejo.

2.4. Supervised Classification

The LULC classes, in the study area, defined by polygons (Regions of Interest—ROIs features) have a uniform distribution [85]. The knowledge of the study area is fundamental to have representative training and validation data samples, for the process of image classification [9]. Thus, for the delimitation of the ROI features, per land use class, we utilized reference data, such as high-resolution satellite images from Google Satellite [86] and the Land Use and Occupation Map (COS) of 2018 from Portugal [87]. When marking the ROI samples, the MetaSearch plugin integrated into QGIS simplifies searching in metadata catalogs compatible with the CSW (Catalog Service for the Web) standard from the Open Geospatial Consortium (OGC) [86]. With a user-friendly interface, the MetaSearch plugin enables access to various services, such as Google Earth Images, facilitating the discovery, navigation, and consultation of geographic metadata [86].

In this study, we defined nine LULC classes, five forest and four non-forest. The five forest classes correspond to five forest species, namely *Eucalyptus* spp., *Pinus pinea*, *Pinus pinaster*, *Quercus rotundifolia*, and *Quercus suber*. The four non-forest classes are as follows: *water surfaces*, *bare soil and artificial surfaces*, *agricultural surface*, and *shrub surface.* We chose to include the bare soil class and urban areas in a single class (bare soil and artificial surfaces). In this study, bare soil and urban areas, as well as agricultural surface classes, were consolidated into single classes, as the primary focus of the research was the classification of major forest covers. During the summer period, the consolidation of agricultural species into a single class was carried out because they exhibit phenological cycles that differ from forest species, resulting in areas of high temporal variability when grouped, which contrasts with the relative stability of forested areas [88]. However, the spectral resolution constraints of Sentinel-2 imagery can present challenges in consistently distinguishing between different crop types [88]. Furthermore, both exposed surfaces bare soil, and urban areas tend to exhibit elevated reflectance values due to low soil moisture content [89] and the presence of artificial materials such as concrete, asphalt, and roofs [90]. This spectral similarity presents challenges in discriminating between these classes, thus supporting their aggregation into a unified category. In this sense, these aggregations reduced the computational complexity of the classification process, allowing for a more efficient and robust analysis, particularly for large-scale studies. In this study, supervised classification was applied using the OTB plugin. The independent stratified

random sampling method was used; 70% of the ROIs were used for training the classifiers, while 30% were used for validation and accuracy assessment [91–93]. The KNN and RF classification algorithms [57] were applied to the 26 independent variables using the OTB 7.1.0 toolkit implemented in the QGIS.

2.4.1. K-Nearest Neighbor and Random Forest Classifiers

This study evaluated and compared the performance of two classifier algorithms: KNN and RF. For the KNN classifier, which has K values ranging from 1 to 35, tests were performed to identify the optimal k value for all training sample sets. The tests revealed an imbalance in accuracies, caused by low K values (overfitting) and very high K values (underfitting), which influenced the performance of the training data [48]. Considering the obtained results, the default value K = 32 defined by OTB was selected for providing a balance between classification accuracy and model generalization. This choice simplifies the process, reduces overfitting effects, balances bias and variance, and ensures classification stability [94,95]. This approach represents a viable alternative for users to initiate the use of the classifier without the need for manual adjustments of this parameter, enabling the achievement of satisfactory classification results [96].

The RF classifier is an algorithm that relies on the configuration of crucial parameters, such as the number of trees, the maximum depth of these trees, and the out-of-bag (OOB) error [97,98]. The optimization of these parameters significantly impacts the model's performance and accuracy [30,41]. The validation dataset was used to generate an unbiased estimate of the error [99]. In this study, the RF model was configured with 500 trees for stability [34,100,101], a maximum depth of 25 to capture complex interactions [102], and an OOB error threshold of 0.01 as a rigorous stopping criterion [34], to maximize classification accuracy and minimize prediction error. This number of trees provides a good balance between processing time and accuracy. Multiple studies [51,88,95,103,104] suggest that increasing the number of trees beyond this point is unlikely to significantly reduce errors.

2.4.2. Accuracy Assessment

By comparing the classified map with the reference image, using the information from the validation samples, accuracy statistics can be derived by the confusion matrix. The confusion matrix is evaluating the degree of errors and classification accuracy in classed maps [105,106]. The confusion matrix assesses the degree of errors and classification accuracy in the classified maps. LULC map accuracy was tested for the overall (OA), producer's (PA), and user's (UA) accuracies and kappa statistics, using the validation dataset (30% of the validation samples) [107,108]. The AO, PA, and UA have been ranked as [101,102] very high (over 90%), high (80–89%), acceptable (70–79%), and low (less than 69%). The kappa coefficient (K) proposed by [109] is most frequently used to test map accuracy. This index is calculated based on the confusion matrix, incorporating both the hits and the omission and commission errors to provide an accurate assessment of agreement [14]. The kappa evaluates the degree of agreement among the classified map and ground truth [110,111]. For a thematic map K > 0.8, the agreement is high [109].

3. Results

3.1. Classification Accuracy

The KNN and RF classification achieved overall accuracy (OA) values greater than 75% for all regions. Both algorithms performed well in terms of classifying the data accurately. However, the RF algorithm stood out for producing OA and k values greater than KNN (approximately 3.5%). The RF algorithm achieved the highest OA value of 92.16% (K = 0.91) in the AC region, while the KNN algorithm had the second highest OA value of 88.69% (K = 0.87) in the same region (Table 3). On the other hand, the minimum values of OA and K were reached in the AG region for both algorithms. Among the NUTS III regions, the AC region had the best classification accuracy with RF and KNN, followed by the AL, BA, AA, and AG regions, in descending order.

Table 3. Overall accuracy (OA) and kappa coefficient (K) assessment of the RF and KNN algorithms.

NUTS III Regions	AC		AL		BA		AA		AG	
Classifiers	**KNN**	**RF**	**KNN**	**RF**	**KNN**	**RF**	**KNN**	**RF**	**KNN**	**RF**
OA (%)	88.69	92.16	83.03	87.49	80.99	86.88	80.25	85.24	75.43	81.86
K	0.87	0.91	0.80	0.86	0.78	0.85	0.77	0.83	0.72	0.79

3.2. Forest Classes Level Accuracy Assessment and Classified Maps

In all regions considered in this study, the classes with other uses, such as *water surfaces* and *bare soil and artificial surfaces*, reached values of UA (commission errors) between 70.81% and 99.92% and values of PA (errors of omission) between 70.11% and 99.54% in both tested classifiers. These results revealed that these sets had a good distinction between forest classes, that is, good spectral separability. Despite the good distinction of the spectral response, this study focuses on evaluating the performance of the classifiers in distinguishing the forest classes. Thus, a deeper evaluation was necessary to understand the contrasts between the forest classes and the reasons for classification errors.

In the forest classes set, the RF classification algorithm was the one that obtained the best PA and UA results in all regions studied (Table 4). The RF algorithm had a PA range from 65.24 to 89.06% and a UA range between 65.47 and 90.00%, while the kNN classifier had a PA range from 54.09 to 84.10% and a UA range from 57.00 to 86.99%. The region that presented the best results for PA and UA was the AC, using the RF classifier. The lowest individual accuracy values between the forest classes were found in the AG region, by both classifiers.

Table 4. Producer (PA) and user (UA) accuracy assessment for the forest classes set obtained by KNN and RF classification.

NUTIII Regions		AC		AL		BA		AA		AG	
Forest Classes	**Accuracy**	**KNN**	**RF**	**KNN**	**RF**	**KNN**	**RF**	**KNN**	**RF**	**KNN**	**RF**
Eucalyptus spp.	PA(%)	81.59	87.85	70.69	77.61	74.38	83.47	77.38	79.14	77.43	85.40
	UA (%)	80.03	88.17	68.91	77.90	73.05	84.25	77.66	80.30	69.27	78.72
Pinus pinea	PA(%)	82.91	89.06	67.44	76.13	80.00	85.33	66.59	81.10	64.96	72.45
	UA (%)	83.97	89.75	77.62	79.90	73.75	80.80	71.98	75.90	65.09	77.05
Pinus pinaster	PA(%)	-	-	74.48	77.80	-	-	75.25	81.15	54.09	67.24
	UA (%)	-	-	68.95	76.27	-	-	79.34	82.75	65.81	72.72
Quercusrotundifolia	PA(%)	82.45	85.79	-	-	64.09	73.61	82.06	84.55	71.63	78.58
	UA (%)	75.53	80.94	-	-	64.87	75.42	68.71	79.69	63.06	71.67
Quercus suber	PA(%)	84.10	86.77	78.31	84.52	69.40	78.22	63.19	74.45	61.28	72.04
	UA (%)	86.99	90.00	70.46	79.51	76.27	82.22	74.13	78.55	57.00	65.47

When verifying the accuracy assessment through visual inspection of the classified map and the reference data, a very similar spatial distribution of forest cover was identified in both maps. In AA and AC regions, the dominant forest cover consisted of *Q. suber* and *Q. rotundifolia*, as *Montado* systems. Additionally, small mosaics of *Eucalyptus* spp. and *P. pinea* were identified, as well as *P. pinaster* stands in the AA region, located within the Serra de São Mamede Natural Park (located in the east of this region (39°18′47″ N; 7°21′36″ W)). In BA region, the predominant cover was spatially dispersed *Q. rotundifolia* with a small concentration of *P. pinea* in the northeast of the region. In the AL region, a higher presence of *P. pinaster* was observed in the coastal region, along with mixed stands of *Q. suber* and *P. pinea* further north. In this region, to the west, there were *Eucalyptus* spp. and *P. pinaster* stands near the Serra de Monchique (located in the west part of this region (37°19′0″ N;

8°33′15″ W)), while a higher spatial distribution of *Q. suber* was found in the central part of the region. The resulting maps from the classification process using KNN and RF, depicting the main forest cover types and other classes, are shown in Figure 3.

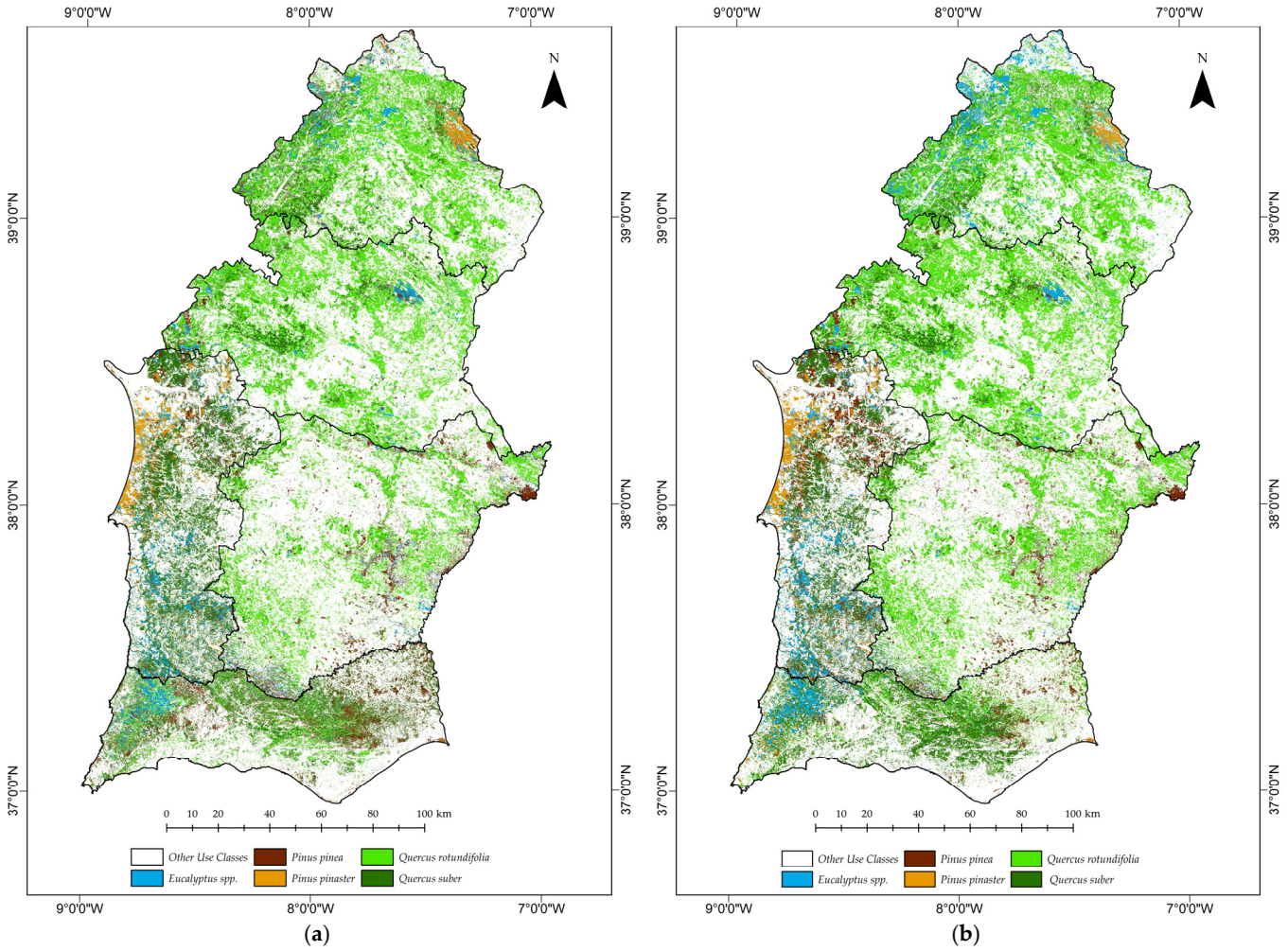

Figure 3. Land use mapping with forest and other uses classes from (**a**) KNN and (**b**) RF algorithms.

In the AC and BA regions, *P. pinaster* occurs in very small patches, making its identification difficult. Therefore, this class was not considered for these two regions under study. The same happens for the species *Q. rotundifolia* in the AL region, where its presence is scarce and dispersed.

4. Discussion

To map the LULC in the NUT III regions, supervised learning algorithms (KNN and RF) were used with a greater focus on the spatial distribution of forest species in complex Mediterranean ecosystems. In the classification step, the same algorithm processing condition (with training and validation datasets) was used to compare the performance of the two algorithms. The accuracy in the production of thematic maps was evaluated by statistical measures obtained by the confusion matrix. The RF algorithm presented greater accuracy and kappa values when compared with the KNN algorithm results, in all regions studied. This was due to its ability to work with numerous input variables, known as big data [112].

Our classification results using the RF algorithm on Sentinel-2 imagery for LULC mapping in the Mediterranean region significantly outperformed those obtained in comparable studies [88,113,114]. For instance, in a classification study conducted at the Köyceğiz Forest

Management Unit, in Turkey, species of *Genista acanthoclada*, *Erica* spp., *Phillyrea latifolia*, *Quercus* spp., *Olea europea*, and *Arbutus andrachne* were classified using Sentinel-2 images using the RF algorithm implemented in the R programing language. The overall accuracy was 78% and kappa 73%, and the accuracies (PA and UA) for each class were greater than 70% [113]. In forest areas located in the eastern part of the Tuscany region, Italy, Sentinel-2 data were evaluated to classify forest classes proposed by [115] in a Mediterranean environment. In the Tuscany region [114], when classifying European Forest Types (EFTs) using the RF classifier, they reached an OA value of 92.7% (k = 92.6%), and for all forest classes, the UA and PA values were greater than 83% using the R programing language. These results reached values close to those found in our work. The reason for these results was that the RF algorithm works better with numerous input variables and is less sensitive to imbalance in training and noise in the training set. Still, other reasons can be cited, for example, it is easy to parameterize, presents good ability to manage collinear resources [116], and is robust against overfitting and outliers [117]. In addition to classification studies in the Mediterranean ecosystem, other authors point to the performance of RF and KNN classifiers on single-date Sentinel-2 images, with good accuracy. Vasilakos et al. [4], using Sentinel-2 data to classify landscapes from the island of Lesbos, Greece, found that when testing six classification algorithms in MATLAB, the KNN and RF classifiers had the better overall accuracy of 89 and 90%, and a kappa coefficient of 86.36% and 87.89%, respectively. In addition, the forest classes evaluated as *Oak* sp., *Pinus brutia*, *Castanea* sp., and *Pinus nigra* did not show great variation in the accuracy values of users and producers [4]. This was an indication that both classifiers may be eligible to produce good forest cover maps.

In comparison with previous studies, our approach utilizing the OTB plugin achieved higher accuracy results, comparable to those developed using programming languages. When mapping LULC with KNN and RF algorithms, both demonstrated good performance, with the RF algorithm yielding higher results. The evaluation metrics of the models, using OTB classifiers, exhibited considerably higher values for overall accuracy and kappa coefficient, evidencing a substantial increase in classification accuracy. Additionally, the obtained producer's accuracy (PA) and user's accuracy (UA) were equivalent to or higher than those reported in the literature, indicating robust consistency across all mapped forest classes.

4.1. Contribution of Independent Variables to Gains in Accuracy

Although our study did not quantitatively assess the relative importance of the independent variables in the classification due to QGIS OTB limitations, the extensive literature review provides solid evidence on the crucial role of these variables in increasing the accuracy of LULC maps. In classification contexts, the exclusive use of spectral bands available in Sentinel-2 often proves insufficient for classifying dense and complex mosaics of different types of forest cover [118]. This is due to the presence of mixed spectral signals from vegetation and similar land covers [119]. Consequently, the incorporation of vegetation and texture indices emerges as a determining factor in accuracy gains in classified maps.

The literature has highlighted the importance of certain Sentinel-2 spectral bands for land use and land cover (LULC) classification, particularly in vegetation classification processes. Previous studies have identified the red, NIR (B8), and SWIR1 (B11) bands as the most significant for mapping different vegetation classes [57,120–122]. The red-edge and SWIR bands have proven crucial for mapping tree species and crop types [88], while the addition of spectral bands with 20 m spatial resolution, resampled to 10 m, allowed for a significant increase in overall accuracy (OA) of single-date classification [120].

The red-edge bands are sensitive to the variability of chlorophyll *a* and *b* [84,122,123], while NIR is sensitive to the variations within and between canopy radiation scattering [57], and SWIR to water content of forest species [124,125]. Other LULC studies have also identified these spectral bands as important variables for classification, especially for forest classes [88,92,126]. In Germany, with SA2S images from one date, the bands with the best predictive ability for forest species were red-edge 1 (B5), SWIR 1 (B11), and the blue band

(B2) [88]. For forests in the Roorkee region, India, the NIR band (B8) of SA2S data from a single date was able to separate forest classes in a range of densities [92]. For *Eucalyptus* spp. species, the bands with the best performance in separating *Eucalyptus* spp. from other land use classes were the green (B3), red-edge 3 (B7) red-edge 4 bands, and/or narrow NIR (B8A) [126].

The inclusion of auxiliary data, such as VIs and textures, is a common approach to formulate a workflow that influences accuracy gains in classification. Our decision to consider certain VIs in this study was based on their demonstrated importance in LULC mapping in Mediterranean ecosystems [127]. From the traditional IVs, SAVI contributed to the soil adjustment constant in the background of the vegetation signal, an important factor when it comes to studies in the dry season and in semi-arid regions [80], and GNDVI, used to estimating photo synthetic activity, thus contributing to separating some forest species [128]. Moreover, EVI showed higher sensitivity in capturing the variability of the canopy in forest systems, due to the changes in namely leaf pigments (chlorophyll and leaf nitrogen) and variability in biomass [82]. The new VIs used in this study, depending on red-edge bands for their calculation, are characterized by lower absorption by chlorophyll, but are sensitive to changes in its content, reducing the saturation effect and enhancing the sensitivity of these VIs to moderate-to-high vegetation densities, reducing the traditional VI saturation effect [16,123]. Research conducted in the Extremadura region of Spain, characterized by Mediterranean vegetation, evaluated multiple spectral indices derived from Sentinel-2 imagery [73]. The study tested various indices, including Brightness Index (BI), Color Index (CI), Green Normalized Difference Vegetation Index (GNDVI), Second Modified Soil-Adjusted Vegetation Index (MSAVI2), Normalized Difference Index (NDI45), Normalized Difference Vegetation Index (NDVI), Normalized Difference Water Index (NDWI), and Soil-Adjusted Vegetation Index (SAVI). In the classification of forest classes using Random Forest algorithms, only CI showed significance. The forest categories included evergreen conifers (*Pinus pinaster*, *Pinus pinea*), dense evergreen broadleaf stands (*Quercus rotundifolia*, *Quercus suber* with canopy cover >60%), sparse evergreen broadleaf areas (20–60% canopy cover), and deciduous broadleaf forests (*Quercus pyrenaica*, *Castanea sativa*), along with nine additional land use classes [73]. Thus, these VIs can contribute to the spectral separability of forest species with proximal spectral response, such as *Q. rotundifolia* and *Q. suber*.

The incorporation of texture indices, specifically GLCM metrics, has also proven valuable in various LULC studies, demonstrating improvements in classification accuracy, as observed in our research [4,101,129,130]. In this study, GLCM proved to have higher sensitivity to the variation of crown cover and abrupt variation in digital numbers neighboring image features, which are predominant in the dry season [131]. Moreover, when studying forest classes with heterogeneous and complex spatial distribution, these bands highlight the contrast at stand boundaries [132,133]. Zheng et al. [68] found that incorporating texture measures into Sentinel-2 spectral data in the RF classification algorithm resulted in a significant increase in LULC accuracy, including in agricultural and vegetation classes. This approach proved effective in mitigating the limitations inherent to pixel-based map classification, addressing the insufficiencies in spatial detail and image sharpness of this algorithm [68].

In the Mediterranean region, Fragoso-Campón et al. [73], investigating the use of a single date for Sentinel data, found that Sentinel-2 texture metrics were very important for optimizing the classification algorithm, especially those derived from visible (B2 and B3), NIR (B5 and B6), and SWIR (B11) bands, which ensured good classification results in the Extremadura region, Spain. Blanco-Sacristán et al. [134] conducted a study using Sentinel-2 data to classify shrub populations in areas affected by historical fires in Sierra Nevada, Spain. In assessing the regeneration process and conservation status of vegetation, the incorporation of textural features derived from GLCM demonstrated a significant contribution to increasing mapping accuracy [134]. Morell-Monzó et al. [135], using very-high-resolution (VHR) images and GLCM textures in mapping abandoned citrus fruits in

Oliva, eastern Spain, found that texture features with a 9 × 9 window size had the best overall accuracy with the Random Forest model.

Other studies conducted by Wang et al. [136] found that textures improved the accuracy of vegetation classification in wetland areas using high-resolution Pléiades satellite images. Feng et al. [137], investigating urban vegetation classification using the RF algorithm and ultra-high-resolution (UHR) digital images obtained by unmanned aerial vehicles (UAVs), highlighted the significant contribution of GLCM textural features in gaining accuracy and eliminating image blurriness, inconsistencies in vegetation classification, and especially the "salt and pepper" effects. Furthermore, the authors observed that the integration of textural metrics compensated for the spectral limitation's characteristic of UAV images [137]. This study highlights the relevance of optical sensors, such as Sentinel-2, in the classification of tree species, based on evidence from the literature. Strategically, it incorporated a set of vegetation indices and textural features to enhance the spectral separability of forest classes and optimize overall classification accuracy. This approach aims to overcome the inherent complexities in classifying Mediterranean forest ecosystems characterized by complex mosaics. The proposed methodology seeks to optimize the application of remote sensing techniques in contexts of high landscape heterogeneity, where precise discrimination of forest classes represents a significant challenge.

Our approach of incorporating vegetation indices and texture, in addition to the standard Sentinel-2 spectral bands, aligns with these findings from the literature. The observed improvement in our classification accuracy suggests that the inclusion of these additional variables played a significant role in enhancing our results obtained from open-source software and plugins.

4.2. The Forest Occupancy Classification Challenges with Images from Sentinel-2

In Mediterranean ecosystems, LULC classification studies using Sentinel-2 images have demonstrated that spectral separability is challenging due to the spectral overlap among pairs of forest classes, *montado* systems, and shrublands, as observed in the autonomous region of Valencia, Spain [138], and among distinct types of broadleaf and coniferous forests in Italy [139]. When it comes to classifying a landscape dominated by fragmented forest stands, remote sensing-based landscape classification remains challenging, as most pixels exhibit similar spectral signatures influenced by ground reflectance or other species and shadows [140,141].

In our study, the classification reliability was verified through visual analysis, comparing the classified map with a reference map, such as high-resolution images from Google Earth. In general, the *Q. rotundifolia* class exhibited several pixels resembling the *Q. suber* class, *shrub* and *agriculture surface*. The mixed species composition in agro-silvopastoral environments and along stand boundaries resulted in categorization errors for *Q. rotundifolia* and *Q. suber* stands in *montado* regions. Particularly in *montado* systems, classifiers might struggle to detect the spatial arrangements of species due to significant variations in mosaic patterns and distribution of forest species [18,142–144]. The spectral similarity between the transition boundaries of regions with center-pivot agriculture, olive groves, and variously oriented vineyard planting lines across all analyzed locations also led to the confusion of some pixels in the *Q. rotundifolia* and *Q. suber* classes. In the AG and BA regions, some *Q. rotundifolia* stands, still young or spatially dispersed in the landscape, had some pixels confused with the *shrub surface* class. The understory vegetation or soils reflectance was reported in other studies in young stands, caused by canopy gaps [145,146]. In the AG region, signatures similar to *Q. suber* were identified within mosaic fragments featuring agricultural surfaces, along with plantations of other crops like *Ficus carica*, *Prunus dulcis*, *Ceratonia siliqua*, and *Citrus* spp.

In regions characterized by steep terrain, situated in AA (Natural Park of Serra de São Mamede), AL (Serra do Cercal), and AG (Serra do Caldeirão and Serra do Monchique), the *P. pinaster* class exhibited a higher classification error along boundaries of the land use patches with *Eucalyptus* spp. stands. In satellite optical imagery, remote sensing techniques

do not account for topographic effects [147,148]. Therefore, our accuracy results might have been influenced by the presence of mountainous areas. Slopes that receive varying sunlight impact the proportion of light returning to the sensor due to changes in solar geometry and topography [149–151]. In these regions, we found greater challenges in defining Regions of Interest (ROIs) due to the vegetation's heterogeneity, comprising other broadleaf species, shrubs, and young cork oaks. For these reasons, there was a heightened spectral confusion between the shrubland class and the *Q. suber* class, which is characteristic of mountainous regions, valley bottoms, north-facing slopes with less solar exposure, and coastal areas (AL and AG). Conversely, the gently undulating relief of the AC region may have contributed to higher accuracy in the LULC classes [152]. These justify the lower accuracy obtained for these regions.

Among the pairs of classes *Q. suber* and *P. pinea*, the confusion between them was nearly equal in the AL region. This is due to the more frequent occurrence of mixed stands of *P. pinea* with *Q. suber* in this region. However, across all studied regions, the classes *Eucalyptus* spp., *P. pinea*, and *P. pinaster* exhibited classification errors due to spectral confusion between riparian species and orchards with similar spectral signatures, as well as mixed stands. The *P. pinea* and *P. pinaster* stands were gradually replaced by *Eucalyptus* spp. due to decreased economic interest in resinous forests and a preference for rapidly growing and economically viable eucalyptus stands [153]. On the other hand, the emergence of mixed areas dominated by pine and eucalyptus reflected the lack of management in *P. pinaster* stands and agricultural abandonment [153]. For these reasons, between the classes of *P. pinaster* and *Eucalyptus* spp., the classifier struggled to delineate the composition of smaller *P. pinaster* mosaics accurately intertwined with larger *Eucalyptus* spp. mosaics. Furthermore, in our study, we identified small fragments of the second rotation of *Eucalyptus* spp., sparse *P. pinaster* stands, and young *P. pinea* plantations that influenced the spectral response due to spatially open canopies and higher reflectance from the ground, rocks, and/or shrub surfaces [154].

The monitoring of land use and land cover (LULC) dynamics is essential for landscape-scale conservation and management. While satellite-based remote sensing constitutes the most feasible approach for large spatial scales, heterogeneous landscapes can pose significant challenges for accurate land cover classification and change detection [155]. A primary obstacle encountered in this study was the classification of forest cover types across extensive territorial expanses, necessitating field expertise, in situ knowledge, visual interpretation of landscape features through ancillary data, and the utilization of high-performance computing resources for image processing. Nonetheless, this investigation addresses a critical gap in the existing literature regarding the large-scale application of algorithmic approaches to LULC analysis in southern Portugal.

Additionally, incorporating multitemporal S2 imagery and leveraging the synergy between Sentinel-1 data, as demonstrated in studies [1,4,156–158], can enhance the classification accuracies of forest occupation classes. Combining texture features extracted from Sentinel-1 (S1) data with Sentinel-2 (S2) multispectral bands enhances classification capabilities. While radar signals from S1 are sensitive to geometric properties (e.g., roughness, texture, and internal structure), optical reflectance from S2 is influenced by vegetation physiology [159,160]. To further improve the non-parametric models used in this research, we propose (1) incorporating additional forest classes, (2) integrating S1 and S2 data into time series, and (3) including new vegetation indices, texture metrics, and elevation features. These enhancements can address existing gaps and potentially increase model accuracy.

5. Conclusions

In this study, we propose an integrative approach to mapping the composition and distribution of the main forest species on a regional scale in southern Portugal, which involves the use of machine learning classification algorithms and free open-source tools. In environmental management and sustainable development, comprehensive mapping of forest land use and cover provides relevant information for developing sustainable

forest management practices, climate change mitigation, managing natural resources, and protecting biodiversity and contributes significantly to improving the accuracy of forest biomass models.

The methodology was developed for mapping forest species using Sentinel-2 data in southern Portugal. The performance of two machine learning algorithms, K-Nearest Neighbor (KNN) and Random Forest (RF) from the OTB plugin, were analyzed to map the main forest species dominating in the five regions of Alentejo and Algarve, Portugal. Despite the complexity of forest species occupancy with high intraclass variability, accurate mapping using OTB plugin classification algorithms was achieved using single Sentinel-2A data.

The RF algorithm achieved the best accuracy results in all evaluated regions when compared to KNN. The best classification accuracies with RF and KNN algorithms were achieved in the AC region (RF: OA = 92.16%, k = 0.91; KNN: OA = 88.69, k = 0.87), followed by AL, BA, AA, and AG. Incorporating ancillary data, such as vegetation and texture indices, into the classification process contributes to the good results obtained. In addition, images acquired in the summer contributed to a good classification due to the lower occurrence of clouds and the distinctive spectral behavior of the understory, as well as between forest classes and other uses. Considering the scale and scope of this investigation, which encompasses the entire southern region of Portugal, the present study significantly expands existing knowledge about the area's forest cover. While previous research has focused on analyses of larger scales [161] or more restricted areas [9], this work fills a crucial gap by providing a more detailed assessment of forest cover across the southern Portuguese region.

The methodology developed in this study offers an efficient and cost-effective approach for producing forest classification maps, utilizing intuitive interface tools like QGIS, SNAP, and the OTB plugin. Sentinel-2 data emerge as a viable and free alternative for large-scale forest classification. Its high spatial and temporal resolution competes with higher-resolution commercial satellite data. Image processing tools from non-commercial software packages facilitate forest species mapping in the Mediterranean ecosystem. These allow users without advanced programming knowledge to achieve good accuracy in their mappings.

Future work perspectives involve expanding the methodology to include classes with lower representation, encompassing the central–northern region of Portugal, and potentially other European regions. Integrating other data sources can help validate the studied model, including field data integration, and merging data from satellites, integrating LiDAR (Light Detection and Ranging) data, high-resolution images obtained from UAVs, and synthetic aperture radar (SAR) data from Sentinel-1. Specifically, integrating LiDAR data, it is worth mentioning that according to the Portuguese Directorate-General for Territory (DGT), the government intends to produce land use and cover maps, as well as hydrography, altimetry, and the Digital Terrain Model based on LiDAR coverage [162]. This project aims to democratize access to national cartographic resources, sharing open data information and integrating cartography resulting from cooperation between various levels of Public Administration.

Author Contributions: C.I. and A.M.O.S. provided the initial concept, research design, data collection, and analysis approach and wrote the manuscript. A.M.C. helped with data collection and analysis approach. A.M.O.S. and A.C.G. helped revise the manuscript. All authors have read and agreed to the published version of the manuscript.

Funding: This work is funded by Programa Operativo de Cooperação Transfronteiriço Espanha-Portugal (POCTEP), project CILIFO—Centro Ibérico para la Investigación y Lucha contra Incendios Forestales (0753_CILIFO_5_E), and by FCT (Foundation for Science and Technology) under the Project with MED (Mediterranean Institute for Agriculture, Environment and Development) (https://doi.org/10.54499/UIDB/05183/2020; https://doi.org/10.54499/UIDP/05183/2020) and CHANGE (Global Change and Sustainability Institute) (https://doi.org/10.54499/LA/P/0121/2020), accessed on 9 December 2024.

Data Availability Statement: The original contributions presented in the study are included in the article, further inquiries can be directed to the corresponding author.

Conflicts of Interest: The authors declare no conflict of interest.

References

1. Chatziantoniou, A.; Psomiadis, E.; Petropoulos, G.P. Co-Orbital Sentinel 1 and 2 for LULC Mapping with Emphasis on Wetlands in a Mediterranean Setting Based on Machine Learning. *Remote Sens.* **2017**, *9*, 1259. [CrossRef]
2. ICNF. *6º Inventário Florestal Nacional (IFN6)*; 2015 Relatório Final; ICNF–Instituto da Conservação da Natureza e das Florestas: Lisboa, Portugal, 2019; p. 284.
3. Peñuelas, J.; Gracia, C.; Jump, A.; Filella, I.; Carnicer, J.; Coll, M.; Lloret, F.; Curiel Yuste, J.; Estiarte, M.; Rutishauser, T.; et al. Introducing the Climate Change Effects on Mediterranean Forest Ecosystems: Observation, Experimentation, Simulation, and Management. *Forêt Médit.* **2010**, *31*, 357–362. Available online: https://hal.science/hal-03573304/ (accessed on 12 November 2024).
4. Vasilakos, C.; Kavroudakis, D.; Georganta, A. Machine Learning Classification Ensemble of Multitemporal Sentinel-2 Images: The Case of a Mixed Mediterranean Ecosystem. *Remote Sens.* **2020**, *12*, 2005. [CrossRef]
5. Di Fazio, S.; Modica, G.; Zoccali, P. Evolution Trends of Land Use/Land Cover in a Mediterranean Forest Landscape in Italy. In Proceedings of the Computational Science and Its Applications-ICCSA 2011, Part I, Lecture Notes in Computer Science, Santander, Spain, 20–23 June 2011; pp. 284–299. [CrossRef]
6. Modica, G.; Merlino, A.; Solano, F.; Mercurio, R. An Index for the Assessment of Degraded Mediterranean Forest Ecosystems. *For. Syst.* **2015**, *24*, 1–13. [CrossRef]
7. Friedl, M.A.; McIver, D.K.; Hodges, J.C.F.; Zhang, X.Y.; Muchoney, D.; Strahler, A.H.; Woodcock, C.E.; Gopal, S.; Schneider, A.; Cooper, A.; et al. Global Land Cover Mapping from MODIS: Algorithms and Early Results. *Remote Sens. Environ.* **2002**, *83*, 287–302. [CrossRef]
8. Isbaex, C.; Coelho, A.M. The potential of Sentinel-2 satellite images for land-cover/land-use and forest biomass estimation: A review. In *Forest Biomass—From Trees to Energy*; Gonçalves, A.C., Sousa, A.M.O., Eds.; IntechOpen: London, UK, 2020; pp. 1–25. [CrossRef]
9. De Luca, G.; Silva, J.M.N.; Cerasoli, S.; Araújo, J.; Campos, J.; Di Fazio, S.; Modica, G. Object-Based Land Cover Classification of Cork Oak Woodlands Using UAV Imagery and Orfeo Toolbox. *Remote Sens.* **2019**, *11*, 1238. [CrossRef]
10. Chen, Y.; Guerschman, J.P.; Cheng, Z.; Guo, L. Remote Sensing for Vegetation Monitoring in Carbon Capture Storage Regions: A Review. *Appl. Energy* **2019**, *240*, 312–326. [CrossRef]
11. ESA. *Sentinel-2 User Handbook*; ESA Standard Document; European Space Agency: Paris, France, 2015; Volume 2, p. 64. [CrossRef]
12. ESA Sentinel Online Spatial Resolution. Available online: https://sentinel.esa.int/web/sentinel/user-guides/sentinel-2-msi/resolutions/spatial (accessed on 12 April 2021).
13. Hawryło, P.; Bednarz, B.; Wężyk, P.; Szostak, M. Estimating Defoliation of Scots Pine Stands Using Machine Learning Methods and Vegetation Indices of Sentinel-2. *Eur. J. Remote Sens.* **2018**, *51*, 194–204. [CrossRef]
14. Mananze, S.; Pôças, I.; Cunha, M. Mapping and Assessing the Dynamics of Shifting Agricultural Landscapes Using Google Earth Engine Cloud Computing, a Case Study in Mozambique. *Remote Sens.* **2020**, *12*, 1279. [CrossRef]
15. Tassi, A.; Vizzari, M. Object-Oriented LULC Classification in Google Earth Learning Algorithms. *Remote Sens.* **2020**, *12*, 3776. [CrossRef]
16. Frampton, W.J.; Dash, J.; Watmough, G.; Milton, E.J. Evaluating the Capabilities of Sentinel-2 for Quantitative Estimation of Biophysical Variables in Vegetation. *ISPRS J. Photogramm. Remote Sens.* **2013**, *82*, 83–92. [CrossRef]
17. Vélez, S.; Martínez-Peña, R.; Castrillo, D. Beyond Vegetation: A Review Unveiling Additional Insights into Agriculture and Forestry through the Application of Vegetation Indices. *J* **2023**, *6*, 421–436. [CrossRef]
18. Godinho, S.; Guiomar, N.; Gil, A. Estimating Tree Canopy Cover Percentage in a Mediterranean Silvopastoral Systems Using Sentinel-2A Imagery and the Stochastic Gradient Boosting Algorithm. *Int. J. Remote Sens.* **2018**, *39*, 4640–4662. [CrossRef]
19. Hall-Beyer, M. Practical Guidelines for Choosing GLCM Textures to Use in Landscape Classification Tasks over a Range of Moderate Spatial Scales. *Int. J. Remote Sens.* **2017**, *38*, 1312–1338. [CrossRef]
20. Haralick, R.M.; Shanmugam, K.; Dinstein, I. Textural Features for Image Classification. *IEEE Trans. Syst. Man. Cybern.* **1973**, *6*, 610–621. [CrossRef]
21. Julesz, B. Experiments in the Visual Perception of Texture. *Sci. Am.* **1975**, *232*, 34–43. [CrossRef] [PubMed]
22. Kupidura, P. The Comparison of Different Methods of Texture Analysis for Their Efficacy for Land Use Classification in Satellite Imagery. *Remote Sens.* **2019**, *11*, 1233. [CrossRef]
23. Colombo, R.; Bellingeri, D.; Fasolini, D.; Marino, C.M. Retrieval of Leaf Area Index in Different Vegetation Types Using High Resolution Satellite Data. *Remote Sens. Environ.* **2003**, *86*, 120–131. [CrossRef]
24. Ferro, C.J.S.; Warner, T.A. Scale and Texture in Digital Image Classification. *Photogramm. Eng. Remote Sens.* **2002**, *68*, 51–63. [CrossRef]
25. Deur, M.; Gašparović, M.; Balenović, I. Tree Species Classification in Mixed Deciduous Forests Using Very High Spatial Resolution Satellite Imagery and Machine Learning Methods. *Remote Sens.* **2020**, *12*, 3926. [CrossRef]

26. Kayitakire, F.; Hamel, C.; Defourny, P. Retrieving Forest Structure Variables Based on Image Texture Analysis and IKONOS-2 Imagery. *Remote Sens. Environ.* **2006**, *102*, 390–401. [CrossRef]
27. Jollife, I.T.; Cadima, J. Principal Component Analysis: A Review and Recent Developments. *Phil. Trans. R. Soc. A* **2016**, *374*, 20150202. [CrossRef]
28. Pinheiro, G.; Minz, S. Granular Computing Based Segmentation and Textural Analysis (GrCSTA) Framework for Object-Based LULC Classification of Fused Remote Sensing Images. *Appl. Intell.* **2024**, *54*, 5748–5767. [CrossRef]
29. Zhao, X.; Jing, L.; Zhang, G.; Zhu, Z.; Liu, H.; Ren, S. Object-Oriented Convolutional Neural Network for Forest Stand Classification Based on Multi-Source Data Collaboration. *Forests* **2024**, *15*, 529. [CrossRef]
30. Liu, P.; Ren, C.; Wang, Z.; Jia, M.; Yu, W.; Ren, H.; Xia, C. Evaluating the Potential of Sentinel-2 Time Series Imagery and Machine Learning for Tree Species Classification in a Mountainous Forest. *Remote Sens.* **2024**, *16*, 293. [CrossRef]
31. Franco-Lopez, H.; Ek, A.R.; Bauer, M.E. Estimation and Mapping of Forest Stand Density, Volume, and Cover Type Using the k-Nearest Neighbors Method. *Remote Sens. Environ.* **2001**, *77*, 251–274. [CrossRef]
32. Moeur, M.; Stage, A.R. Most Similar Neighbor: An Improved Sampling Inference Procedure for Natural Resource Planning. *Forest Sci.* **1995**, *41*, 337–359. [CrossRef]
33. Cover, T.M.; Hart, P.E. Nearest Neighbor Pattern Classification. *IEEE Trans. Inf. Theory* **1967**, *13*, 21–27. [CrossRef]
34. Breiman, L. Random Forests. *Mach. Learn.* **2001**, *45*, 5–32. [CrossRef]
35. Wettschereck, D.; Aha, D.W.; Mohri, T. A Review and Empirical Evaluation of Feature Weighting Methods for a Class of Lazy Learning Algorithms. *Artif. Intell. Rev.* **1997**, *11*, 273–314. [CrossRef]
36. Duda, R.; Hart, P. *Pattern Classification and Scene Analysis*; John Wiley & Sons: New York, NY, USA, 1973.
37. Akbulut, Y.; Sengur, A.; Guo, Y.; Smarandache, F. NS-k-NN: Neutrosophic Set-Based k-Nearest Neighbors Classifier. *Symmetry* **2017**, *9*, 179. [CrossRef]
38. Qian, Y.; Zhou, W.; Yan, J.; Li, W.; Han, L. Comparing Machine Learning Classifiers for Object-Based Land Cover Classification Using Very High Resolution Imagery. *Remote Sens.* **2015**, *7*, 153–168. [CrossRef]
39. Wei, C.; Huang, J.; Mansaray, L.R.; Li, Z.; Liu, W.; Han, J. Estimation and Mapping of Winter Oilseed Rape LAI from High Spatial Resolution Satellite Data Based on a Hybrid Method. *Remote Sens.* **2017**, *9*, 488. [CrossRef]
40. Dorigo, W.; Lucieer, A.; Podobnikar, T.; Carni, A. Mapping Invasive Fallopia Japonica by Combined Spectral, Spatial, and Temporal Analysis of Digital Orthophotos. *Int. J. Appl. Earth Obs. Geoinf.* **2012**, *19*, 185–195. [CrossRef]
41. Hu, Y.; Xu, X.; Wu, F.; Sun, Z.; Xia, H.; Meng, Q.; Huang, W.; Zhou, H.; Gao, J.; Li, W.; et al. Estimating Forest Stock Volume in Hunan Province, China, by Integrating In Situ Plot Data, Sentinel-2 Images, and Linear and Machine Learning Regression Models. *Remote Sens.* **2020**, *12*, 186. [CrossRef]
42. European Space Agency (ESA). Sentinel Application Platform—SNAP. Available online: https://step.esa.int/main/download/snap-download/ (accessed on 6 May 2021).
43. Hernandez, I.; Benevides, P.; Costa, H.; Caetano, M. Exploring Sentinel-2 for Land Cover and Crop Mapping in Portugal. *Int. Arch. Photogramm. Remote Sens. Spat. Inf. Sci.* **2020**, *43*, 83–89. [CrossRef]
44. Gislason, P.O.; Benediktsson, J.A.; Sveinsson, J.R. Random Forests for Land Cover Classification. *Pattern Recognit. Lett.* **2006**, *27*, 294–300. [CrossRef]
45. Jin, Y.; Liu, X.; Chen, Y.; Liang, X. Land-Cover Mapping Using Random Forest Classification and Incorporating NDVI Time-Series and Texture: A Case Study of Central Shandong. *Int. J. Remote Sens.* **2018**, *39*, 8703–8723. [CrossRef]
46. Praticò, S.; Solano, F.; Di Fazio, S.; Modica, G. Machine Learning Classification of Mediterranean Forest Habitats in Google Earth Engine Based on Seasonal Sentinel-2 Time-Series and Input Image Composition Optimisation. *Remote Sens.* **2021**, *13*, 586. [CrossRef]
47. Ouma, Y.O.; Gabasiane, T.G.; Nkhwanana, N. Mapping Prosopis L. (Mesquites) Using Sentinel-2 MSI Satellite Data, NDVI and SVI Spectral Indices with Maximum-Likelihood and Random Forest Classifiers. *J. Sens.* **2023**, *2023*, 18. [CrossRef]
48. Thanh Noi, P.; Kappas, M. Comparison of Random Forest, k-Nearest Neighbor, and Support Vector Machine Classifiers for Land Cover Classification Using Sentinel-2 Imagery. *Sensors* **2018**, *18*, 18. [CrossRef]
49. Lu, D.; Weng, Q. A Survey of Image Classification Methods and Techniques for Improving Classification Performance. *Int. J. Remote Sens.* **2007**, *28*, 823–870. [CrossRef]
50. Gómez, C.; White, J.C.; Wulder, M.A. Optical Remotely Sensed Time Series Data for Land Cover Classification: A Review. *ISPRS J. Photogramm. Remote Sens.* **2016**, *116*, 55–72. [CrossRef]
51. Rodriguez-Galiano, V.F.; Ghimire, B.; Rogan, J.; Chica-Olmo, M.; Rigol-Sanchez, J.P. An Assessment of the Effectiveness of a Random Forest Classifier for Land-Cover Classification. *ISPRS J. Photogramm. Remote Sens.* **2012**, *67*, 93–104. [CrossRef]
52. Papadopoulou, E.; Mallinis, G.; Siachalou, S.; Koutsias, N.; Thanopoulos, A.C.; Tsaklidis, G. Agricultural Land Cover Mapping through Two Deep Learning Models in the Framework of EU's CAP Activities Using Sentinel-2 Multitemporal Imagery. *Remote Sens.* **2023**, *15*, 4657. [CrossRef]
53. Kycko, M.; Zagajewski, B.; Kluczek, M.; Tardà, A.; Pineda, L.; Palà, V.; Corbera, J. Sentinel-2 and AISA Airborne Hyperspectral Images for Mediterranean Shrubland Mapping in Catalonia. *Remote Sens.* **2022**, *14*, 5531. [CrossRef]
54. Valdivieso-Ros, C.; Alonso-Sarria, F.; Gomariz-Castillo, F. Effect of the Synergetic Use of Sentinel-1, Sentinel-2, LiDAR and Derived Data in Land Cover Classification of a Semiarid Mediterranean Area Using Machine Learning Algorithms. *Remote Sens.* **2023**, *15*, 312. [CrossRef]

55. Abida, K.; Barbouchi, M.; Boudabbous, K.; Toukabri, W.; Saad, K.; Bousnina, H.; Sahli Chahed, T. Sentinel-2 Data for Land Use Mapping: Comparing Different Supervised Classifications in Semi-Arid Areas. *Agriculture* **2022**, *12*, 1429. [CrossRef]
56. Orfeo ToolBox (OTB). Available online: https://www.orfeo-toolbox.org/ (accessed on 30 April 2022).
57. Cresson, R.; Grizonnet, M.; Michel, J. Orfeo ToolBox Applications. In *QGIS and Generic Tools*; John Wiley & Sons, Inc.: Hoboken, NJ, USA, 2018; pp. 151–242. [CrossRef]
58. Grizonnet, M.; Michel, J.; Poughon, V.; Inglada, J.; Savinaud, M.; Cresson, R. Orfeo ToolBox: Open Source Processing of Remote Sensing Images. *Open Geospat. Data Softw. Stand.* **2017**, *2*, 15. [CrossRef]
59. Gabinete de Estratégia e Estudos. Nut II/Nut IIII. Categorias. Available online: https://www.gee.gov.pt/pt/documentos/publicacoes/estatisticas-regionais/nut-ii-nut-iii (accessed on 30 April 2022).
60. Sousa, A.M.O.; Gonçalves, A.C.; da Silva, J.R.M. Above-Ground Biomass Estimation with High Spatial Resolution Satellite Images. In *Biomass Volume Estimation and Valorization for Energy*; IntechOpen: London, UK, 2017; pp. 1–24. [CrossRef]
61. Pinto-Correia, T.; Ribeiro, N.; Sá-Sousa, P. Introducing the Montado, the Cork and Holm Oak Agroforestry System of Southern Portugal. *Agrofor. Syst.* **2011**, *82*, 99–104. [CrossRef]
62. Barrico, L.; Rodríguez-Echeverría, S.; Freitas, H. Diversity of Soil Basidiomycete Communities Associated with *Quercus Suber* L. in Portuguese Montados. *Eur. J. Soil Biol.* **2010**, *46*, 280–287. [CrossRef]
63. Gonçalves, A.C.; Sousa, A.M.O.; Mesquita, P.G. Estimation and Dynamics of Above Ground Biomass with Very High Resolution Satellite Images in *Pinus pinaster* stands. *Biomass Bioenergy* **2017**, *106*, 146–154. [CrossRef]
64. Sandim, A.; Silva, M.E.; Gonçalves, A.C.; Tomé, M.; Fonseca, T.F. Management of *Pinus pinaster* Aiton for Wood and Resin Production: A Technical-Financial Feasibility Analysis. In *Conifers-Recent Advances*; IntechOpen: London, UK, 2022; pp. 1–20. [CrossRef]
65. *National Forestry Accounting Plan Portugal 2021–2025*; Governo de Portugal, Agência Portuguesa de Ambiente: Lisboa, Portugal, 2020; pp. 1–80.
66. Sousa, J.L.C.; Ramos, P.A.B.; Freire, C.S.R.; Silva, A.M.S.; Silvestre, A.J.D. Chemical Composition of Lipophilic Bark Extracts from *Pinus Pinaster* and *Pinus Pinea* Cultivated in Portugal. *Appl. Sci.* **2018**, *8*, 2575. [CrossRef]
67. Martínez-Chico, M.; Batlles, F.J.; Bosch, J.L. Cloud Classification in a Mediterranean Location Using Radiation Data and Sky Images. *Energy* **2011**, *36*, 4055–4062. [CrossRef]
68. Zheng, H.; Du, P.; Chen, J.; Xia, J.; Li, E.; Xu, Z.; Li, X.; Yokoya, N. Performance Evaluation of Downscaling Sentinel-2 Imagery for Land Use and Land Cover Classification by Spectral-Spatial Features. *Remote Sens.* **2017**, *9*, 1274. [CrossRef]
69. Wiesmair, M.; Feilhauer, H.; Magiera, A.; Otte, A.; Waldhardt, R. Estimating Vegetation Cover from High-Resolution Satellite Data to Assess Grassland Degradation in the Georgian Caucasus. *Mt. Res. Dev.* **2016**, *36*, 56–65. [CrossRef]
70. Jensen, J.R. *Remote Sensing of the Environment: An Earth Resource Perspective*; Prentice Hall: Upper Saddle River, NJ, USA, 2006.
71. Eklundh, L.; Singh, A. A Comparative Analysis of Standardised and Unstandardised Principal Components Analysis in Remote Sensing. *Int. J. Remote Sens.* **1993**, *14*, 1359–1370. [CrossRef]
72. Waser, L.T.; Küchler, M.; Jütte, K.; Stampfer, T. Evaluating the Potential of Worldview-2 Data to Classify Tree Species and Different Levels of Ash Mortality. *Remote Sens.* **2014**, *6*, 4515–4545. [CrossRef]
73. Fragoso-Campón, L.; Quirós, E.; Gallego, J.A.G. Optimization of Land Cover Mapping through Improvements in Sentinel-1 and Sentinel-2 Image Dimensionality and Data Mining Feature Selection for Hydrological Modeling. *Stoch. Environ. Res. Risk Assess.* **2021**, *35*, 2493–2519. [CrossRef]
74. Franklin, S.E.; Hall, R.J.; Moskal, L.M.; Maudie, A.J.; Lavigne, M.B. Incorporating Texture into Classification of Forest Species Composition from Airborne Multispectral Images. *Int. J. Remote Sens.* **2000**, *21*, 61–79. [CrossRef]
75. Szantoi, Z.; Escobedo, F.; Abd-Elrahman, A.; Smith, S.; Pearlstine, L. Analyzing Fine-Scale Wetland Composition Using High Resolution Imagery and Texture Features. *Int. J. Appl. Earth Obs. Geoinf.* **2013**, *23*, 204–212. [CrossRef]
76. Huang, C.; Zhang, C.; He, Y.; Liu, Q.; Li, H.; Su, F.; Liu, G.; Bridhikitti, A. Land Cover Mapping in Cloud-Prone Tropical Areas Using Sentinel-2 Data: Integrating Spectral Features with Ndvi Temporal Dynamics. *Remote Sens.* **2020**, *12*, 1163. [CrossRef]
77. De Fioravante, P.; Luti, T.; Cavalli, A.; Giuliani, C.; Dichicco, P.; Marchetti, M.; Chirici, G.; Congedo, L.; Munafò, M. Multispectral Sentinel-2 and Sar Sentinel-1 Integration for Automatic Land Cover Classification. *Land* **2021**, *10*, 611. [CrossRef]
78. Chaves, M.E.D.; Soares, A.R.; Mataveli, G.A.V.; Sánchez, A.H.; Sanches, I.D. A Semi-Automated Workflow for LULC Mapping via Sentinel-2 Data Cubes and Spectral Indices. *Automation* **2023**, *4*, 94–109. [CrossRef]
79. Gitelson, A.A.; Kaufman, Y.J.; Merzlyak, M.N. Use of a Green Channel in Remote Sensing of Global Vegetation from EOS- MODIS. *Remote Sens. Environ.* **1996**, *58*, 289–298. [CrossRef]
80. Huete, A.R. A Soil-Adjusted Vegetation Index (SAVI). *Remote Sens. Environ.* **1988**, *25*, 295–309. [CrossRef]
81. Hunt, E.R.; Rock, B.N. Detection of Changes in Leaf Water Content Using Near- and Middle-Infrared Reflectances. *Remote Sens. Environ.* **1989**, *30*, 43–54. [CrossRef]
82. Liu, H.Q.; Huete, A. Feedback Based Modification of the NDVI to Minimize Canopy Background and Atmospheric Noise. *IEEE Trans. Geosci. Remote Sens.* **1995**, *33*, 457–465. [CrossRef]
83. Navarro, G.; Caballero, I.; Silva, G.; Parra, P.C.; Vázquez, Á.; Caldeira, R. Evaluation of Forest Fire on Madeira Island Using Sentinel-2A MSI Imagery. *Int. J. Appl. Earth Obs. Geoinf.* **2017**, *58*, 97–106. [CrossRef]

84. Zarco-Tejada, P.J.; Miller, J.R.; Noland, T.L.; Mohammed, G.H.; Sampson, P.H. Scaling-up and Model Inversion Methods with Narrowband Optical Indices for Chlorophyll Content Estimation in Closed Forest Canopies with Hyperspectral Data. *IEEE Trans. Geosci. Remote Sens.* **2001**, *39*, 1491–1507. [CrossRef]
85. Ma, L.; Li, M.; Ma, X.; Cheng, L.; Du, P.; Liu, Y. A Review of Supervised Object-Based Land-Cover Image Classification. *ISPRS J. Photogramm. Remote Sens.* **2017**, *130*, 277–293. [CrossRef]
86. Documentation QGIS. MetaSearch Catalog Plugin. 2021. Available online: https://plugins.qgis.org/plugins/MetaSearch/ (accessed on 1 July 2023).
87. Divisão Geral do Território—DGT. Carta de Uso e Ocupação do Solo—COS 2018. 2020. Available online: https://www.dgterritorio.gov.pt/Carta-de-Uso-e-Ocu (accessed on 1 July 2023).
88. Immitzer, M.; Vuolo, F.; Atzberger, C. First Experience with Sentinel-2 Data for Crop and Tree Species Classifications in Central Europe. *Remote Sens.* **2016**, *8*, 166. [CrossRef]
89. Liu, Y.; Meng, Q.; Zhang, L.; Wu, C. NDBSI: A Normalized Difference Bare Soil Index for Remote Sensing to Improve Bare Soil Mapping Accuracy in Urban and Rural Areas. *Catena* **2022**, *214*, 106265. [CrossRef]
90. Hofierka, J.; Onačillová, K. Estimating Visible Band Albedo from Aerial Orthophotographs in Urban Areas. *Remote Sens.* **2022**, *14*, 164. [CrossRef]
91. Adam, E.; Mutanga, O.; Odindi, J.; Abdel-Rahman, E.M. Land-Use/Cover Classification in a Heterogeneous Coastal Landscape Using RapidEye Imagery: Evaluating the Performance of Random Forest and Support Vector Machines Classifiers. *Int. J. Remote Sens.* **2014**, *35*, 3440–3458. [CrossRef]
92. Saini, R.; Ghosh, S.K. Crop Classification on Single Date Sentinel-2 Imagery Using Random Forest and Suppor Vector Machine. *Int. Arch. Photogramm. Remote Sens. Spat. Inf. Sci.* **2018**, *XLII–5*, 683–688. [CrossRef]
93. Lim, J.; Kim, K.M.; Jin, R. Tree Species Classification Using Hyperion and Sentinel-2 Data with Machine Learning in South Korea and China. *ISPRS Int. J. Geo-Inf.* **2019**, *8*, 150. [CrossRef]
94. Pal, M. Random Forest Classifier for Remote Sensing Classification. *Int. J. Remote Sens.* **2005**, *26*, 217–222. [CrossRef]
95. Maxwell, A.E.; Warner, T.A.; Fang, F. Implementation of Machine-Learning Classification in Remote Sensing: An Applied Review. *Int. J. Remote Sens.* **2018**, *39*, 2784–2817. [CrossRef]
96. Jombo, S.; Adelabu, S. Evaluating Landsat-8, Landsat-9 and Sentinel-2 Imageries in Land Use and Land Cover (LULC) Classification in a Heterogeneous Urban Area. *GeoJournal* **2023**, *88*, 377–399. [CrossRef]
97. Chabalala, Y.; Adam, E.; Ali, K.A. Machine Learning Classification of Fused Sentinel-1 and Sentinel-2 Image Data towards Mapping Fruit Plantations in Highly Heterogenous Landscapes. *Remote Sens.* **2022**, *14*, 2621. [CrossRef]
98. Kluczek, M.; Zagajewski, B.; Zwijacz-Kozica, T. Mountain Tree Species Mapping Using Sentinel-2, PlanetScope, and Airborne HySpex Hyperspectral Imagery. *Remote Sens.* **2023**, *15*, 844. [CrossRef]
99. Breiman, L.; Friedman, J.H.; Olshen, R.A.; Stone, C.J. *Classification and Regression Trees*; Chapman & Hall: New York, NY, USA, 1984; pp. 1–17. ISBN 9780412048418.
100. Billah, M.; Islam, A.K.M.S.; Bin Mamoon, W.; Rahman, M.R. Random Forest Classifications for Landuse Mapping to Assess Rapid Flood Damage Using Sentinel-1 and Sentinel-2 Data. *Remote Sens. Appl. Soc. Environ.* **2023**, *30*, 100947. [CrossRef]
101. Fu, Y.; Tan, H.; Kou, W.; Xu, W.; Wang, H.; Lu, N. Estimation of Rubber Plantation Biomass Based on Variable Optimization from Sentinel-2 Remote Sensing Imagery. *Forests* **2024**, *15*, 900. [CrossRef]
102. Hastie, T.; Tibshirani, R.; Friedman, J. Random forests. In *The Elements of Statistical Learning*; Springer: Berlin/Heidelberg, Germany, 2009; pp. 587–604. [CrossRef]
103. Huang, B.F.F.; Boutros, P.C. The Parameter Sensitivity of Random Forests. *BMC Bioinform.* **2016**, *17*, 331. [CrossRef]
104. Mellor, A.; Haywood, A.; Stone, C.; Jones, S. The Performance of Random Forests in an Operational Setting for Large Area Sclerophyll Forest Classification. *Remote Sens.* **2013**, *5*, 2838–2856. [CrossRef]
105. FAO—Food and Agriculture Organization of the United Nations. *Map Accuracy Assessment and Area Estimation: A Practical Guide*; FAO: Rome, Italy, 2016; Volume E, pp. 1–55.
106. Xiong, J.; Thenkabail, P.S.; Tilton, J.C.; Gumma, M.K.; Teluguntla, P.; Oliphant, A.; Congalton, R.G.; Yadav, K.; Gorelick, N. Nominal 30-m Cropland Extent Map of Continental Africa by Integrating Pixel-Based and Object-Based Algorithms Using Sentinel-2 and Landsat-8 Data on Google Earth Engine. *Remote Sens.* **2017**, *9*, 1065. [CrossRef]
107. Story, M.; Congalton, R.G. Remote Sensing Brief Accuracy Assessment: A User's Perspective. *Photogramm. Eng. Remote Sens.* **1986**, *52*, 397–399. Available online: https://www.asprs.org/wp-content/uploads/pers/1986journal/mar/1986_mar_397-399.pdf (accessed on 30 April 2022).
108. Phiri, D.; Simwanda, M.; Salekin, S.; Ryirenda, V.R.; Murayama, Y.; Ranagalage, M.; Oktaviani, N.; Kusuma, H.A.; Zhang, T.; Su, J.; et al. Remote Sensing Sentinel-2 Data for Land Cover/Use Mapping: A Review. *Remote Sens.* **2019**, *42*, 2219. [CrossRef]
109. Landis, J.R.; Koch, G.G. The Measurement of Observer Agreement for Categorical Data. *Int. Biom. Soc.* **1977**, *33*, 159–174. [CrossRef]
110. Manfré, L.A.; De Albuquerque Nóbrega, R.A.; Quintanilha, J.A. Evaluation of Multiple Classifier Systems for Landslide Identification in LANDSAT Thematic Mapper (TM) Images. *ISPRS Int. J. Geo-Inf.* **2016**, *5*, 164. [CrossRef]
111. Foody, G.M.; Mathur, A. Toward Intelligent Training of Supervised Image Classifications: Directing Training Data Acquisition for SVM Classification. *Remote Sens. Environ.* **2004**, *93*, 107–117. [CrossRef]

112. Boateng, E.Y.; Otoo, J.; Abaye, D.A.; Boateng, E.Y.; Otoo, J.; Abaye, D.A. Basic Tenets of Classification Algorithms K-Nearest-Neighbor, Support Vector Machine, Random Forest and Neural Network: A Review. *J. Data Anal. Inf. Process.* **2020**, *8*, 341–357. [CrossRef]
113. Çağlayan, S.D.; Leloglu, U.M.; Ginzler, C.; Psomas, A.; Zeydanlı, U.S.; Bilgin, C.C.; Waser, L.T. Species Level Classification of Mediterranean Sparse Forests-Maquis Formations Using Sentinel-2 Imagery. *Geocarto Int.* **2020**, *37*, 1587–1606. [CrossRef]
114. Puletti, N.; Chianucci, F.; Castaldi, C. Use of Sentinel-2 for Forest Classification in Mediterranean Environments. *Ann. Silvic. Res.* **2017**, *42*, 32–38. [CrossRef]
115. Barbati, A.; Marchetti, M.; Chirici, G.; Corona, P. European Forest Types and Forest Europe SFM Indicators: Tools for Monitoring Progress on Forest Biodiversity Conservation. *For. Ecol. Manag.* **2014**, *321*, 145–157. [CrossRef]
116. Pelletier, C.; Valero, S.; Inglada, J.; Champion, N.; Dedieu, G. Assessing the Robustness of Random Forests to Map Land Cover with High Resolution Satellite Image Time Series over Large Areas. *Remote Sens. Environ.* **2016**, *187*, 156–168. [CrossRef]
117. Liaw, A.; Wiener, M. Classification and Regression by RandomForest. *R News* **2002**, *2*, 18–22.
118. Gutkin, N.; Uwizeyimana, V.; Somers, B.; Muys, B.; Verbist, B. Supervised Classification of Tree Cover Classes in the Complex Mosaic Landscape of Eastern Rwanda. *Remote Sens.* **2023**, *15*, 2606. [CrossRef]
119. Nandasena, W.D.K.V.; Brabyn, L.; Serrao-Neumann, S. Using Google Earth Engine to Classify Unique Forest and Agroforest Classes Using a Mix of Sentinel 2a Spectral Data and Topographical Features: A Sri Lanka Case Study. *Geocarto Int.* **2022**, *37*, 9544–9559. [CrossRef]
120. Pouliot, D.A.; King, D.J.; Bell, F.W.; Pitt, D.G. Automated Tree Crown Detection and Delineation in High-Resolution Digital Camera Imagery of Coniferous Forest Regeneration. *Remote Sens. Environ.* **2002**, *82*, 322–334. [CrossRef]
121. Zarco-Tejada, P.J.; Hornero, A.; Beck, P.S.A.; Kattenborn, T.; Kempeneers, P.; Hernández-Clemente, R. Chlorophyll Content Estimation in an Open-Canopy Conifer Forest with Sentinel-2A and Hyperspectral Imagery in the Context of Forest Decline. *Remote Sens. Environ.* **2019**, *223*, 320–335. [CrossRef] [PubMed]
122. Adamczyk, J.; Osberger, A. Red-Edge Vegetation Indices for Detecting and Assessing Disturbances in Norway Spruce Dominated Mountain Forests. *Int. J. Appl. Earth Obs. Geoinf.* **2015**, *37*, 90–99. [CrossRef]
123. Clevers, J.G.P.W.; Gitelson, A.A. Remote Estimation of Crop and Grass Chlorophyll and Nitrogen Content Using Red-Edge Bands on Sentinel-2 and-3. *Int. J. Appl. Earth Obs. Geoinf.* **2013**, *23*, 344–351. [CrossRef]
124. Bolyn, C.; Michez, A.; Gaucher, P.; Lejeune, P.; Bonnet, S. Forest Mapping and Species Composition Using Supervised per Pixel Classification of Sentinel-2 Imagery. *Biotechnol.Agron. Soc. Environ.* **2018**, *22*, 172–187. [CrossRef]
125. Rautiainen, M.; Lukeš, P.; Homolová, L.; Hovi, A.; Pisek, J.; Mõttus, M. Spectral Properties of Coniferous Forests: A Review of in Situ and Laboratory Measurements. *Remote Sens.* **2018**, *10*, 207. [CrossRef]
126. Sibanda, M.; Mutanga, O.; Rouget, M. Examining the Potential of Sentinel-2 MSI Spectral Resolution in Quantifying above Ground Biomass across Different Fertilizer Treatments. *ISPRS J. Photogramm. Remote Sens.* **2015**, *110*, 55–65. [CrossRef]
127. Fragoso-Campón, L.; Quirós, E.; Mora, J.; Gallego, J.A.G.; Durán-Barroso, P. Overstory-Understory Land Cover Mapping at the Watershed Scale: Accuracy Enhancement by Multitemporal Remote Sensing Analysis and LiDAR. *Environ. Sci. Pollut. Res.* **2020**, *27*, 75–88. [CrossRef]
128. Pesaresi, S.; Mancini, A.; Quattrini, G.; Casavecchia, S. Evaluation and Selection of Multi-Spectral Indices to Classify Vegetation Using Multivariate Functional Principal Component Analysis. *Remote Sens.* **2024**, *16*, 1224. [CrossRef]
129. Solymosi, K.; Kövér, G.; Romvári, R. The Progression of Vegetation Indices: A Short Overview. *Acta Agrar. Kaposváriensis* **2019**, *23*, 75–90. [CrossRef]
130. Schulz, C.; Förster, M.; Vulova, S.V.; Rocha, A.D.; Kleinschmit, B. Spectral-Temporal Traits in Sentinel-1 C-Band SAR and Sentinel-2 Multispectral Remote Sensing Time Series for 61 Tree Species in Central Europe. *Remote Sens. Environ.* **2024**, *307*, 114162. [CrossRef]
131. Trong, H.N.; Nguyen, T.D.; Kappas, M. Land Cover and Forest Type Classification by Values of Vegetation Indices and Forest Structure of Tropical Lowland Forests in Central Vietnam. *Int. J. For. Res.* **2020**. [CrossRef]
132. Numbisi, F.N.; Van Coillie, F.; De Wulf, R. Multi-date Sentinel 1 SAR image textures discriminate perennial agroforests in a tropical forest-savanna transition landscape. *Int. Arch. Photogramm. Remote Sens. Spat. Inf. Sci.* **2018**, *42*, 339–346. [CrossRef]
133. Park, Y.; Guldmann, J.M. Measuring Continuous Landscape Patterns with Gray-Level Co-Occurrence Matrix (GLCM) Indices: An Alternative to Patch Metrics? *Ecol. Indic.* **2020**, *109*, 105802. [CrossRef]
134. Blanco-Sacristán, J.; Guirado, E.; Molina-Pardo, J.L.; Cabello, J.; Giménez-Luque, E.; Alcaraz-Segura, D. Remote Sensing-Based Monitoring of Postfire Recovery of Persistent Shrubs: The Case of Juniperus Communis in Sierra Nevada (Spain). *Fire* **2023**, *6*, 4. [CrossRef]
135. Morell-Monzó, S.; Sebastiá-Frasquet, M.T.; Estornell, J. Land Use Classification of Vhr Images for Mapping Small-Sized Abandoned Citrus Plots by Using Spectral and Textural Information. *Remote Sens.* **2021**, *13*, 681. [CrossRef]
136. Wang, X.; Wang, S.; Dai, L. Estimating and Mapping Forest Biomass in Northeast China Using Joint Forest Resources Inventory and Remote Sensing Data. *J. For. Res.* **2018**, *29*, 797–811. [CrossRef]
137. Feng, Q.; Liu, J.; Gong, J. UAV Remote Sensing for Urban Vegetation Mapping Using Random Forest and Texture Analysis. *Remote Sens.* **2015**, *7*, 1074–1094. [CrossRef]

138. Campos-Taberner, M.; Javier García-Haro, F.; Martínez, B.; Sánchez-Ruiz, S.; Moreno-Martínez, Á.; Camps-Valls, G.; Amparo Gilabert, M. Land Use Classification over Smallholding Areas in the European Common Agricultural Policy Framework. *ISPRS J. Photogramm. Remote Sens.* **2023**, *197*, 320–334. [CrossRef]
139. Agrillo, E.; Filipponi, F.; Pezzarossa, A.; Casella, L.; Smiraglia, D.; Orasi, A.; Attorre, F.; Taramelli, A. Earth Observation and Biodiversity Big Data for Forest Habitat Types Classification and Mapping. *Remote Sens.* **2021**, *13*, 1231. [CrossRef]
140. Fassnacht, F.E.; Latifi, H.; Stereńczak, K.; Modzelewska, A.; Lefsky, M.; Waser, L.T.; Straub, C.; Ghosh, A. Review of Studies on Tree Species Classification from Remotely Sensed Data. *Remote Sens. Environ.* **2016**, *186*, 64–87. [CrossRef]
141. Grabska, E.; Hostert, P.; Pflugmacher, D.; Ostapowicz, K. Forest Stand Species Mapping Using the Sentinel-2 Time Series. *Remote Sens.* **2019**, *11*, 1197. [CrossRef]
142. Coelho, A.M.; Sousa, A.M.O.; Gonçalves, A.C. Spatial Variability of Forest Species: Case Study for Alto Alentejo, Portugal. *Land* **2023**, *12*, 46. [CrossRef]
143. Sousa, A.M.O.; Gonçalves, A.C.; Mesquita, P.; Marques da Silva, J.R. Biomass Estimation with High Resolution Satellite Images: A Case Study of Quercus Rotundifolia. *ISPRS J. Photogramm. Remote Sens.* **2015**, *101*, 69–79. [CrossRef]
144. Macedo, F.L.; Sousa, A.M.O.; Gonçalves, A.C.; Marques da Silva, J.R.; Mesquita, P.A.; Rodrigues, R.A.F. Above-Ground Biomass Estimation for Quercus Rotundifolia Using Vegetation Indices Derived from High Spatial Resolution Satellite Images. *Eur. J. Remote Sens.* **2018**, *51*, 932–944. [CrossRef]
145. Joyce, S.; Olsson, H. Monitoring Forest Growth Using Long Time Series of Satellite Data. *Int. Arch. Photogramm. Remote Sens.* **2000**, *33*, 1081–1088.
146. Nilson, T.; Rautiainen, M.; Pisek, J.; Peterso, U. Seasonal Reflectance Courses of Forests. In *New Adv. Contribut. Forest. Res.*; IntechOpen: London, UK, 2012; pp. 33–58. [CrossRef]
147. Stohr, C.J.; West, T.R. Terrain and Look Angle Effects Upon I Multispectral Scanner Response. *Photogramm. Eng. Remote Sens.* **1985**, *51*, 229–235. Available online: https://www.asprs.org/wp-content/uploads/pers/1985journal/feb/1985_feb_229-235.pdf (accessed on 30 April 2022).
148. Teillet, P.M. Image Correction for Radiometric Effects in Remote Sensing. *Int. J. Remote Sens.* **1986**, *7*, 1637–1651. [CrossRef]
149. Hugli, H.; Frei, W. Understanding Anisotropic Reflectance in Mountainous Terrain. *Photogramm. Eng. Remote Sens.* **1983**, *49*, 671–683. Available online: https://www.asprs.org/wp-content/uploads/pers/1983journal/may/1983_may_671-683.pdf (accessed on 30 April 2022).
150. Teillet, P.M.; Guindon, B.; Goodenough, D.G. On the Slope-Aspect Correction of Multispectral Scanner Data. *Can. J. Remote Sens.* **1982**, *8*, 84–106. [CrossRef]
151. Hosciło, A.; Lewandowska, A. Mapping Forest Type and Tree Species on a Regional Using Multi-Temporal Sentinel-2 Data. *Remote Sens.* **2019**, *11*, 929. [CrossRef]
152. Dados.gov. Hipsometria de Portugal Continental. Available online: https://dados.gov.pt/pt/datasets/hipsometria-de-portugal-continental/ (accessed on 8 July 2024).
153. Lomba, A.; Vicente, J.; Moreira, F.; Honrado, J. Effects of Multiple Factors on Plant Diversity of Forest Fragments in Intensive Farmland of Northern Portugal. *For. Ecol. Manag.* **2011**, *262*, 2219–2228. [CrossRef]
154. Akbari, V.; Solberg, S.; Puliti, S. Multitemporal Sentinel-1 and Sentinel-2 Images for Characterization and Discrimination of Young Forest Stands under Regeneration in Norway. *IEEE J. Sel. Top. Appl. Earth Obs. Remote Sens.* **2021**, *14*, 5049–5063. [CrossRef]
155. Allen, H.; Simonson, W.; Parham, E.; Santos, E.D.B.E.; Hotham, P. Satellite Remote Sensing of Land Cover Change in a Mixed Agro-Silvo-Pastoral Landscape in the Alentejo, Portugal. *Int. J. Remote Sens.* **2018**, *39*, 4663–4683. [CrossRef]
156. Nelson, M. Evaluating Multitemporal Sentinel-2 Data for Forest Mapping Using Random Forest. Master's Thesis, Stockholm University, Stockholm, Sweden, 2017.
157. Tavares, P.A.; Beltrão, N.E.S.; Guimarães, U.S.; Teodoro, A.C. Integration of Sentinel-1 and Sentinel-2 for Classification and LULC Mapping in the Urban Area of Belém, Eastern Brazilian Amazon. *Sensors* **2019**, *19*, 1140. [CrossRef]
158. Mngadi, M.; Odindi, J.; Peerbhay, K.; Mutanga, O. Examining the Effectiveness of Sentinel-1 and 2 Imagery for Commercial Forest Species Mapping. *Geocarto Int.* **2021**, *36*, 1–12. [CrossRef]
159. Dobrinić, D.; Gašparović, M.; Medak, D. Sentinel-1 and 2 Time-Series for Vegetation Mapping Using Random Forest Classification: A Case Study of Northern Croatia. *Remote Sens.* **2021**, *13*, 2321. [CrossRef]
160. Mercier, A.; Betbeder, J.; Rumiano, F.; Baudry, J.; Al, E. Evaluation of Sentinel-1 and 2 Time Series for Land Cover Classification of Forest–Agriculture Mosaics in Temperate and Tropical Landscapes. *Remote Sens.* **2019**, *11*, 979. [CrossRef]
161. Malinowski, R.; Lewiński, S.; Rybicki, M.; Gromny, E.; Jenerowicz, M.; Krupiński, M.; Nowakowski, A.; Wojtkowski, C.; Krupiński, M.; Krätzschmar, E.; et al. Automated Production of a Land Cover/Use Map of Europe Based on Sentinel-2 Imagery. *Remote Sens.* **2020**, *12*, 3523. [CrossRef]
162. Gabinete da Ministra da Coesão Territorial. Portaria n.º 377/2024/2. Diário da República n.49, S. 2, 8 de março de 2024. Available online: https://files.diariodarepublica.pt/2s/2024/03/049000000/0006300065.pdf (accessed on 8 July 2024).